Supporting Information

Photocatalytic C-C coupling reactions of benzyl alcohol for hydrobenzoin over Z-scheme $ZnS/ZnIn_2S_4$

Xinyu Jin,[a] Chun Cai.[*a]

[a] School of Chemistry and Chemical Engineering, Nanjing University of Science & Technology, Xiaolingwei 200, Nanjing 210094, P. R. China.
[*]E-mail: c.cai@njust.edu.cn

Experiment section: Characterizations, Calculation of the band gap energy (E_g).

Table S1. Chemical compositions of $ZnIn_2S_4$ and $ZnS/ZnIn_2S_4$ hybrids obtained from ICP-MS.

Table S2. Structural properties of $ZnIn_2S_4$, $ZnS/ZnIn_2S_4$-2 and ZnS.

Table S3. Comparison of the selective benzyl alcohol C-C coupling performance over different photocatalysts.

Table S4. The results of control experiments for studying the reaction mechanism.

Table S5. The selective coupling of different aldehyde with ZnS/ $ZnIn_2S_4$-2 as the photocatalyst.

Fig. S1 (a) XRD patterns of the ZnS and (b) XRD patterns of six samples.

Fig. S2 HR-TEM image of (a) $ZnIn_2S_4$ (b) ZnS (c) $ZnS/ZnIn_2S_4$-2.

Fig. S3 SAED patterns of (a) $ZnIn_2S_4$ (b) ZnS (c) ZnS/ $ZnIn_2S_4$-2

Fig. S4 EPR spectra of DMPO-ketyl radical for ZnS, $ZnIn_2S_4$ and $ZnS/ZnIn_2S_4$-2.

Fig. S5 Light absorption of I_3^- (typical absorbance at 350 nm) in the solution after photocatalytic reaction with addition of excess KI to detect the produced H_2O_2.

Data for C-C coupling products of aryl alcohols.

^{1}H NMR for C-C coupling products of aryl alcohols.

Experimental section

Characterizations. X-ray diffraction (XRD) patterns were performed using a Rigaku smartlab9 (40KV, 150mA) with Cu Kα radiation. The morphology and crystal phase of the samples were characterized using field emission transmission electron microscopy (FETEM, FEI Talos F200x), scanning electron microscopeand (SEM, FEI Nova NanoSEM 450), high-resolution transmission electron microscopy (HRTEM, FEI Talos F200x) with selected area electron diffraction (SAED). The elemental composition was investigated by energy-dispersive X-ray spectroscopy (EDX, FEI Talos F200x). UV-vis diffuse reflectance spectroscopy (DRS) was measured on a Shimadzu UV-3600plus, and collected data was converted from reflection to absorbance using the Kubelka-Munk function. X-ray photoelectron spectroscopy (XPS) data was performed on an ESCALAB 250Xi spectrometer, using an Al Kα X-ray source (1350 eV of photons) and calibrated by setting the C 1s peak to 284.80 eV. Inductively coupled plasma mass spectrometry (ICP-MS) was analyzed on Optima 7300 DV. The BET surface area and pore size measurements were performed with N_2 adsorption/desorption isotherms at 77 K on a Micromeritics ASAP 2020 instrument. Before measurements, the samples were degassed at 80 °C for 12 h. Electron paramagnetic resonance (EPR) measurements were performed on a Bruker A300 EPR EMX Nano Spectrometer. The electrochemical and photoelectrochemical analysis was conducted on an electrochemical workstation (CHI1660E, Shanghai Chenhua Science Technology Co., Ltd.) with a conventional three-electrode cell, which used a Pt plate as the counter electrode, a $BiVO_4$ film as the working electrode and a saturated silver chloride electrode as the reference electrode. The electrochemical impedance spectroscopy (EIS) measurements were measured in the presence of 0.2 M Na_2SO_4 solution in a frequency range from 0.1 Hz to 100 kHz under open circuit potential conditions. The photocurrent responses were measured in the presence of saturated KCl solution with Ag/AgCl as the reference electrode and the initial voltage was 0.7 V. The photoluminescence (PL) was analyzed on HORIBA HR Evolution with an excitation wavelength of 325 nm. GC-MS was performed on an ISQ Trace 1300 in the electron ionization (EI) mode. GC analyses are performed on an Agilent 7890A instrument (Column: Agilent 19091J-413: 30 m × 320 μm × 0.25 μm, carrier gas: H_2, FID detection. The surface photovoltage spectroscopy (SPV) was measured by a stable surface photovoltage spectrometer (PL-SPV/IPCE 1000, Beijing Perfectlight Technology Co.,Ltd.).

Calculation of the band gap energy (E_g). Since ZnS and $ZnIn_2S_4$ is belonged to the direct band gap semiconductors, the following formula is used to calculate the E_g of $ZnIn_2S_4$:

$$(\alpha hv)^n = K \times (hv\text{-}E_g)$$

where α is the absorption coefficient, hv is the photon energy, K is a constant, E_g is the band gap energy and n is 2 because ZnS and $ZnIn_2S_4$ belongs to direct semiconductor.

Table S1. Chemical compositions of $ZnIn_2S_4$ and $ZnS/ZnIn_2S_4$ hybrids obtained from ICP-MS.

Sample	Atomic%			Weight%			Zn: In: S (Atomic)
	Zn	In	S	Zn	In	S	
$ZnIn_2S_4$	21.18	47.29	31.53	13.85	54.3	31.85	0.45:1:0.67
$ZnS/ZnIn_2S_4$-1	36.9	35.23	27.87	24.12	40.45	35.43	1.05:1:0.79
$ZnS/ZnIn_2S_4$-2	41.14	24.14	34.72	26.9	27.72	45.38	1.70:1:1.44
$ZnS/ZnIn_2S_4$-3	48.56	22.16	29.28	31.75	25.44	42.81	2.19:1:1.32
$ZnS/ZnIn_2S_4$-4	48.42	16.05	35.53	31.66	18.43	49.91	3.02:1:2.22

Table S2. Structural properties of $ZnIn_2S_4$, $ZnS/ZnIn_2S_4$-2 and ZnS.

Samples	BET surface area (m^2/g)	Pore volume (cm^3/g)	Average pore size (nm)
ZnS	8.89	0.045	27.76
$ZnIn_2S_4$	69.15	0.196	12.05
ZnS/ $ZnIn_2S_4$-2	113.75	0.3111	11.59
NV-ZnS/ $ZnIn_2S_4$-2	92.93	0.1179	6.36

Table S3. Comparison of the selective benzyl alcohol C-C coupling performance over different photocatalysts.

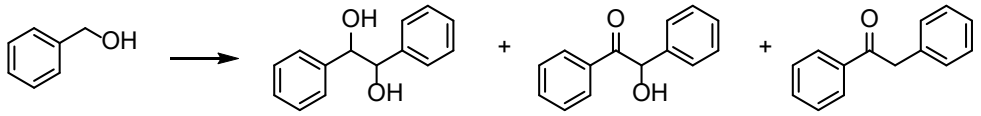

1a 2a 3a 4a

Entry	Photocatalyst	Reaction condition	1a Con. (%)	Selectivity (%)			
				2a	3a	4a	Others (aldehyde)
1	CTAB/$ZnIn_2S_4$[1]	9.6 mM BAL, CH_3CN, Ar, 7h, λ=455 nm (6 W blue LEDs)	99		69		31
2	Ag_2S/CdS[2]	100 mM BAL, CH_3CN, Ar,4h, λ=445 nm (6 W blue LEDs)	100	-	-	97	3
3	Ag/CdS[3]	100 mM BAL, CH_3CN, Ar, 4h, λ=445 nm (6 W blue LEDs)	100		95		5
4	CdS /$Zn_2In_2S_5$[4]	192 mM BAL, CH_3CN, N_2, 2h, λ> 400 nm (300W Xe lamp)	33		96		4
5	$Zn_{0.6}In_2S_{3.6}$[5]	200 mM BAL, CH_3CN, Ar, 6h, λ=455 nm (6 W blue LEDs)	99	-	16	64	20
6	CdS QDs[6]	2 mM BAL, H_2O/D_2O, Ar, 10h, λ=405nm	100	49	-	8	43
7	$ZnIn_2S_4$[7]	10 mM BAL, CH_3CN (70 vol% H_2O), N_2, 10h, λ=440~460 nm	100	2	58	40	-
8	Ni@$ZnIn_2S_4$[8]	15 mM BAL, CH_3CN, N_2, 2h, 300W Xe lamp	86	99	-	-	-
9	CdS/TiO_2[9]	20 mM BAL, CH_3CN, CO_2, 2h, λ > 420 nm	28	95	-	-	5
10	HC-CdS2/Co[10]	24 mM BAL, CH_3CN, Ar, 9h, λ=420 nm	92	97	-	-	-
11	DTAB/$ZnIn_2S_4$[11]	70 mM BAL, CH_3CN, N_2, 11h, λ > 400 nm (300 W Xe lamp)	99	54	31	12	-
12	$ZnIn_2S_4$-P[12]	90 mM BAL, DMF, N_2, 6h, λ=455 nm (blue LEDs)	95	81	7	-	12
13	ZnS/$ZnIn_2S_4$-2 (This work)	96 mM BAL, DMF (10 vol% H_2O), air, 2h, λ=415 nm (12 W LEDs)	100	92	5	1	2

Table S4. The results of control experiments for studying the reaction mechanism. [a]

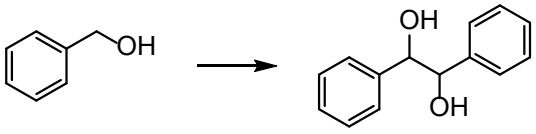

Benzyl alcohol(BAL) Hydrobenzoin(HB)

Entry	Photocatalyst	Light	BAL Con.[b] (%)	HB Sel.[b] (%)
1	$ZnS/ZnIn_2S_4$-2	415 nm	100	93
2	/	415 nm	0	-
3	$ZnS/ZnIn_2S_4$-2	/	0	-

[a] Reaction conditions: 10 mg $ZnS/ZnIn_2S_4$-2, 5 mL solvent: DMF (10 vol% H_2O), 0.48 mmol Benzyl alcohol, 415 nm, air, 2 h. [b] the data were obtained by GC.

Table S5. The selective coupling of different aldehyde with $ZnS/ZnIn_2S_4$-2 as the photocatalyst. [a]

Entry	Substrate	Con.[b] (%)	Selectivity [b] (%)			
			2a	3a	4a	Others(aldehyde)
1	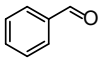	99	65	3	1	31
2	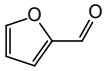	100	98	1	1	0

[a] Reaction conditions: 10 mg $ZnS/ZnIn_2S_4$-2, 5 mL solvent: DMF (10 vol% H_2O), 0.48 mmol substrates, 415 nm, air, 8 h. [b] the data were obtained by GC.

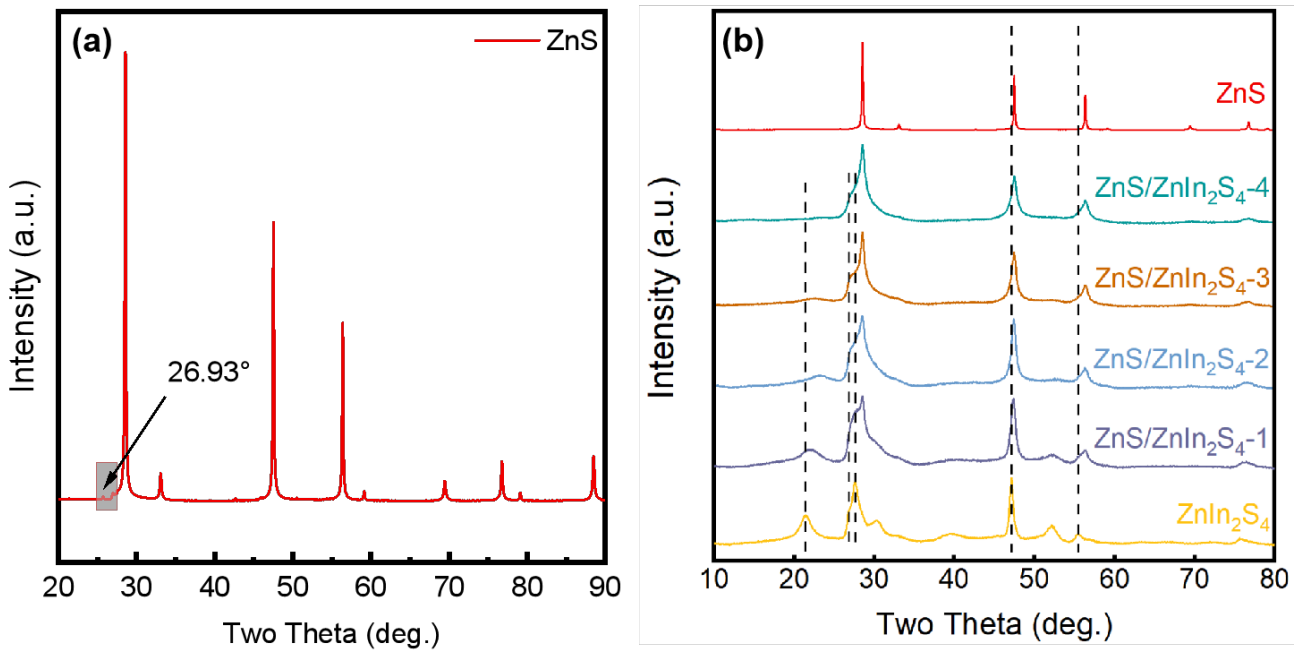

Fig. S1 (a) XRD patterns of the ZnS and (b) XRD patterns of six samples.

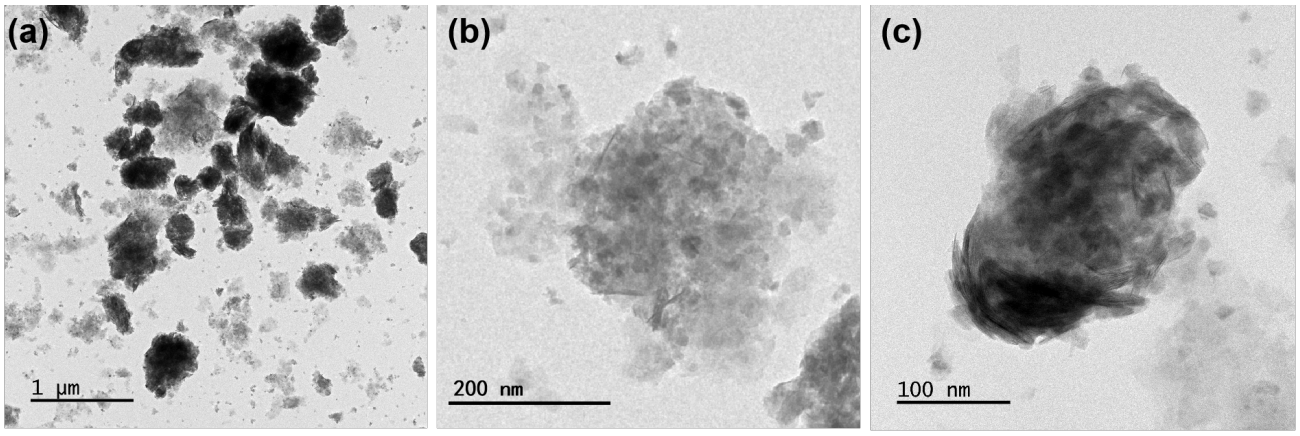

Fig. S2 TEM image of $ZnS/ZnIn_2S_4$-2.

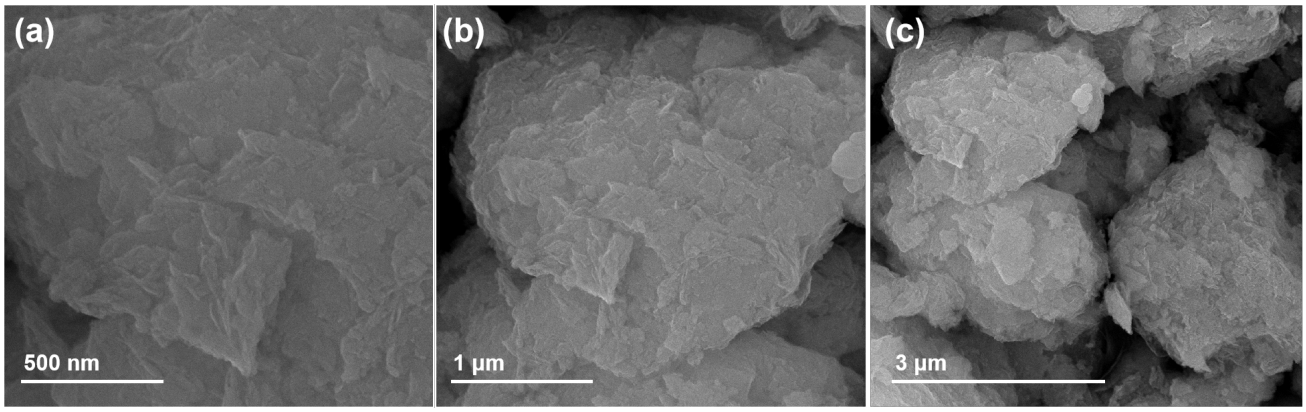

Fig. S3 SEM image of $ZnS/ZnIn_2S_4$-2.

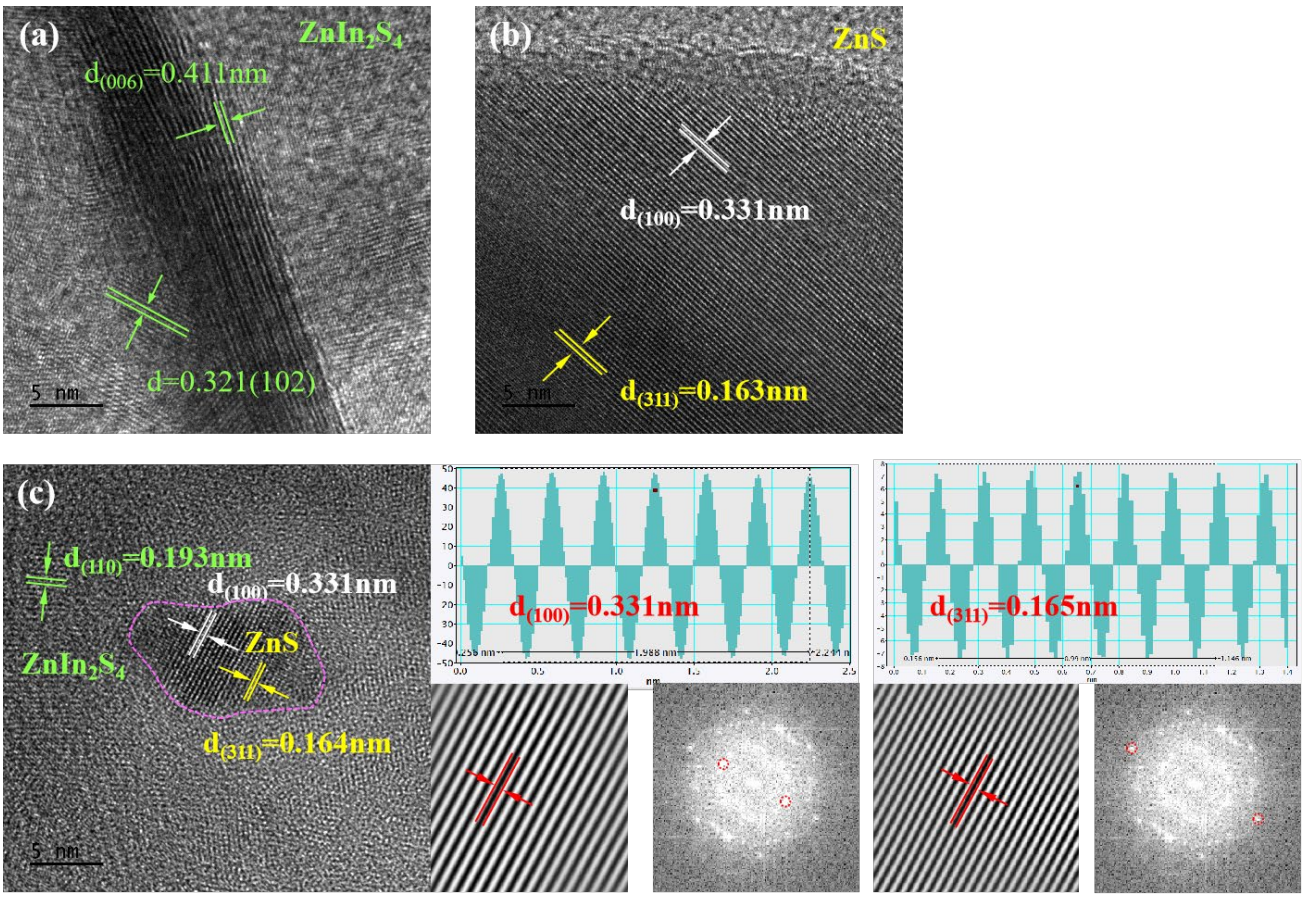

Fig. S4 HRTEM image of (a) $ZnIn_2S_4$ (b) ZnS (c) $ZnS/ZnIn_2S_4$-2.

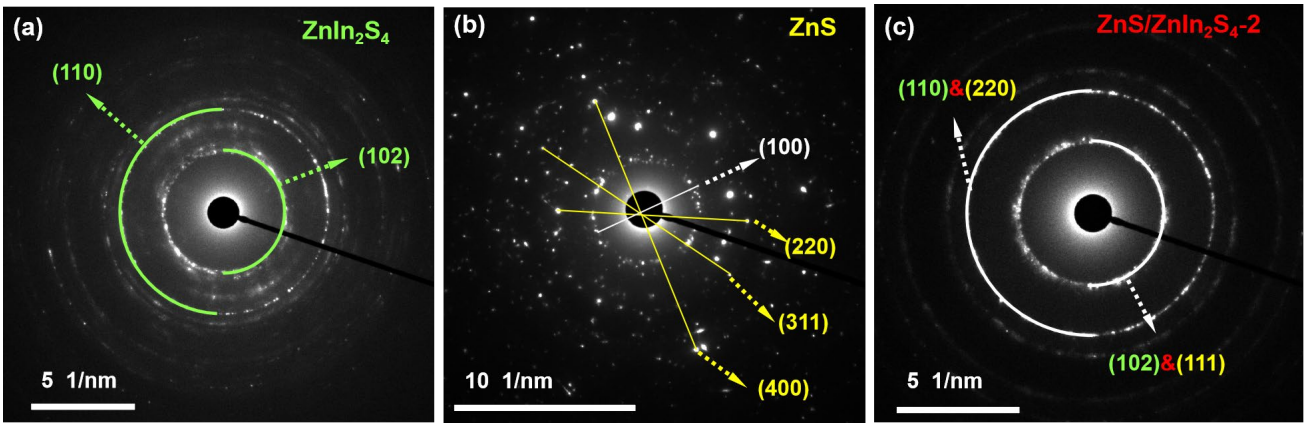

Fig. S5 SAED patterns of (a) $ZnIn_2S_4$ (b) ZnS (c) $ZnS/ZnIn_2S_4$-2.

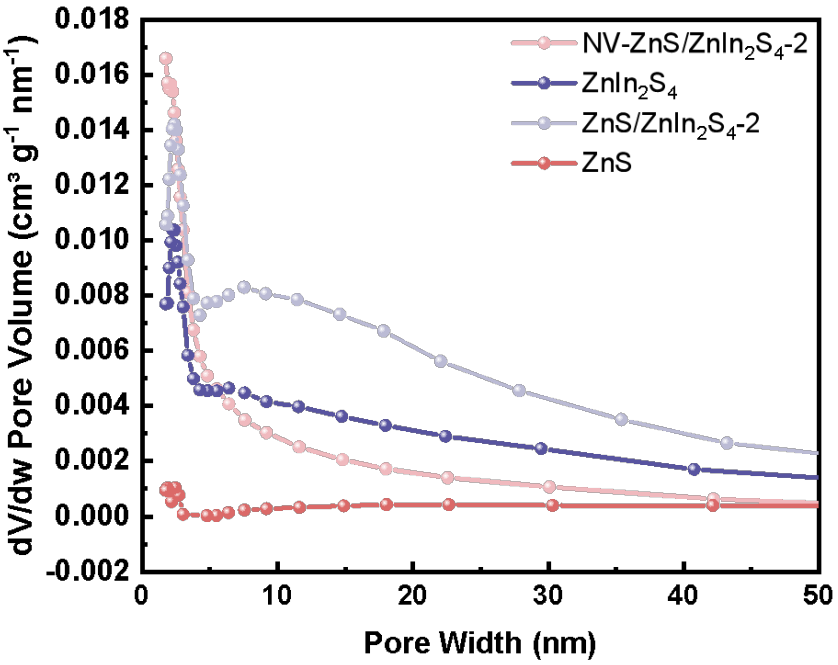

Fig. S6 The BJH pore size distribution curve of $ZnIn_2S_4$, ZnS, $ZnS/ZnIn_2S_4$-2 and NV-$ZnS/ZnIn_2S_4$-2.

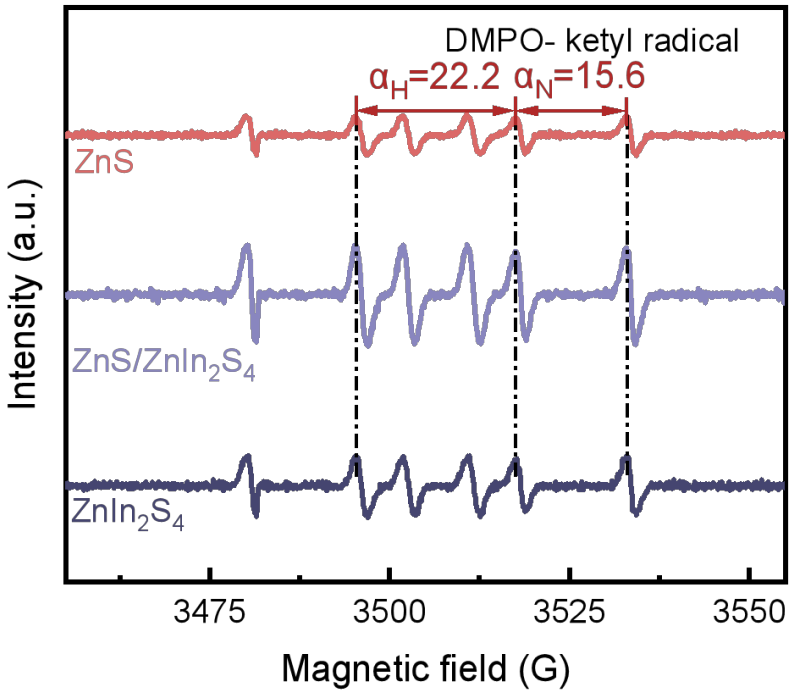

Fig. S7 EPR spectra of DMPO-ketyl radical for ZnS, $ZnIn_2S_4$ and $ZnS/ZnIn_2S_4$-2.

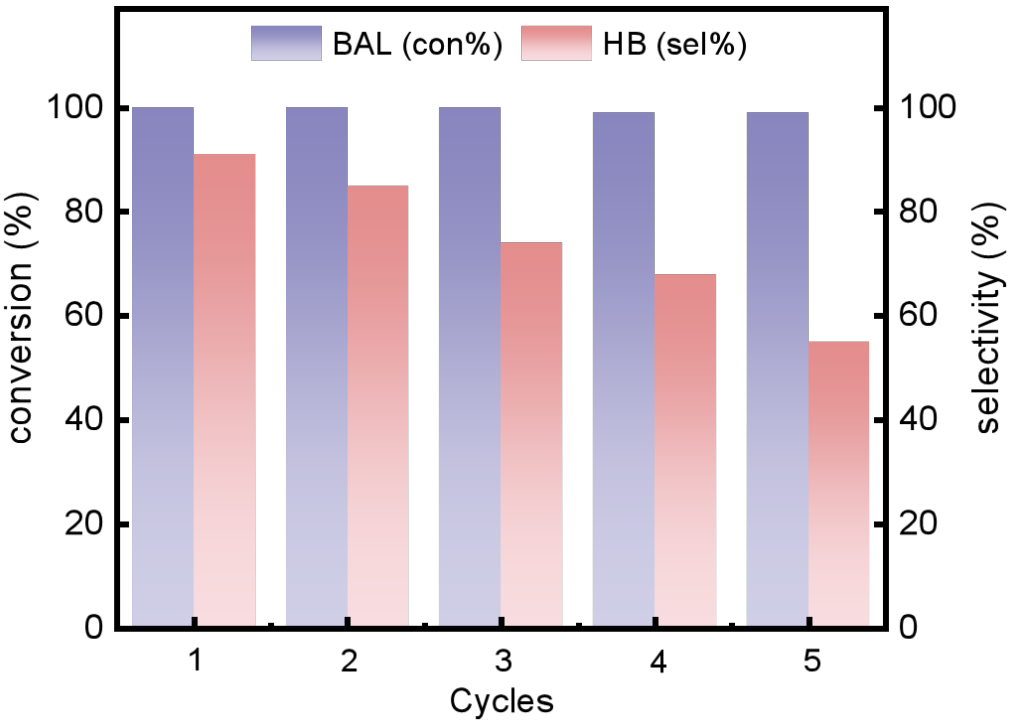

Fig. S8 Stability test of ZnS/$ZnIn_2S_4$-2. Reaction conditions: 0.48mmol benzyl alcohol, 10 mg photocatalyst in 5 ml solvent under 415 nm LED irradiation for 2 h in air at room temperature.

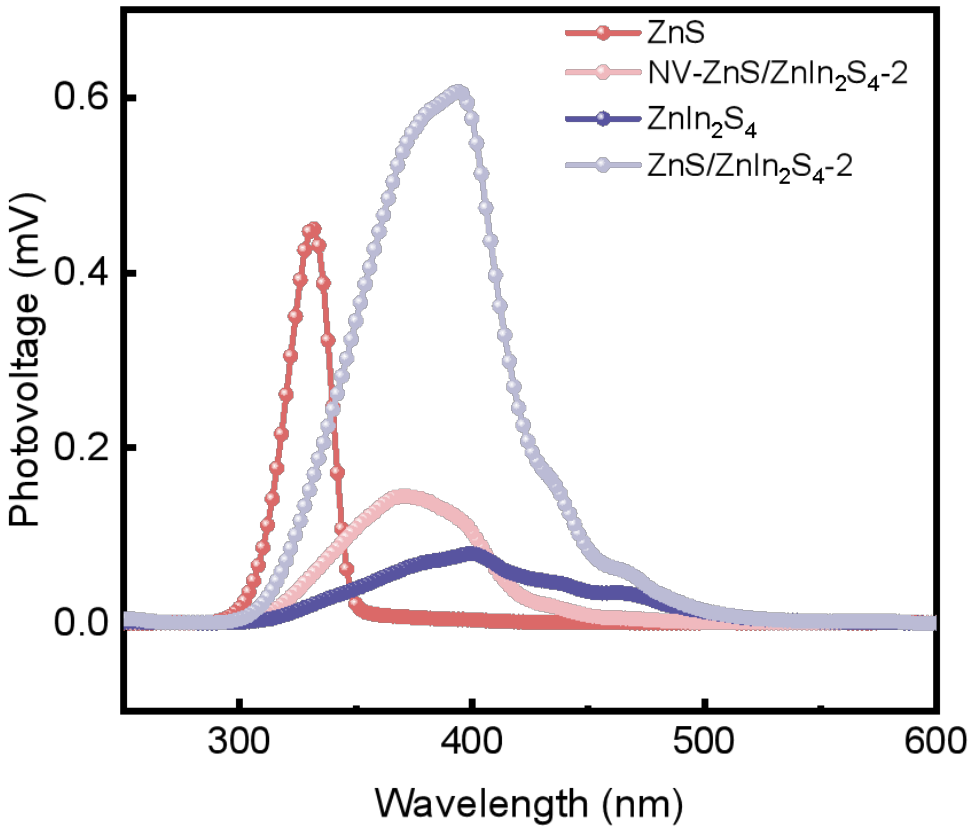

Fig. S9 SPV spectra of ZnS, $ZnIn_2S_4$, ZnS/$ZnIn_2S_4$-2 and NV-ZnS/$ZnIn_2S_4$-2.

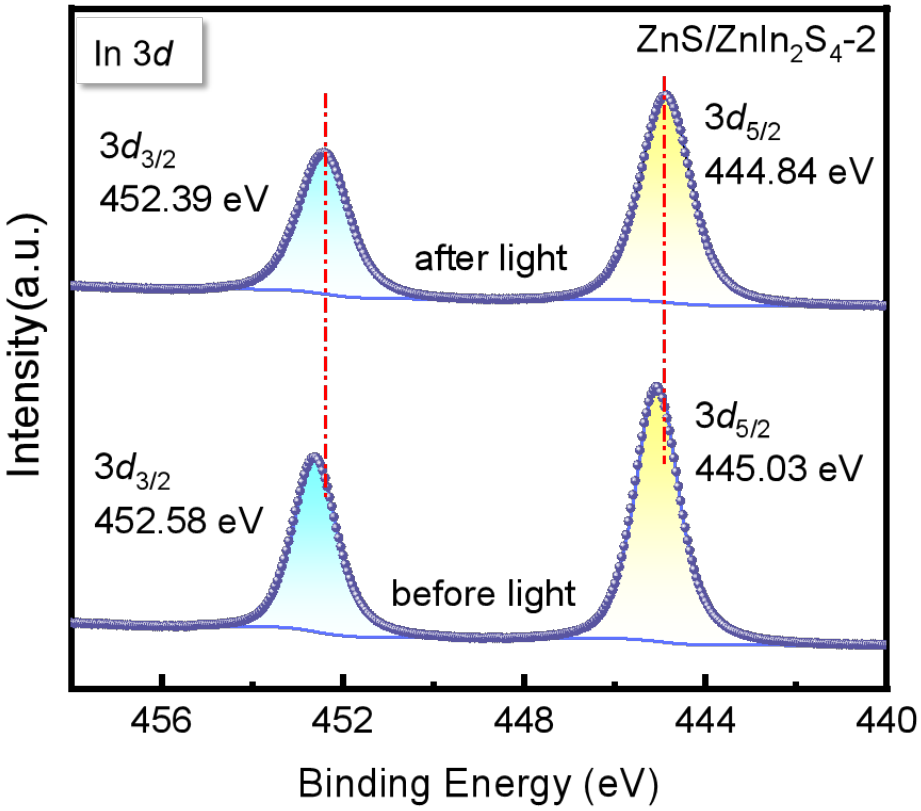

Fig. S10 In-situ XPS spectra of In of $ZnS/ZnIn_2S_4$-2 sample before and after light illumination.

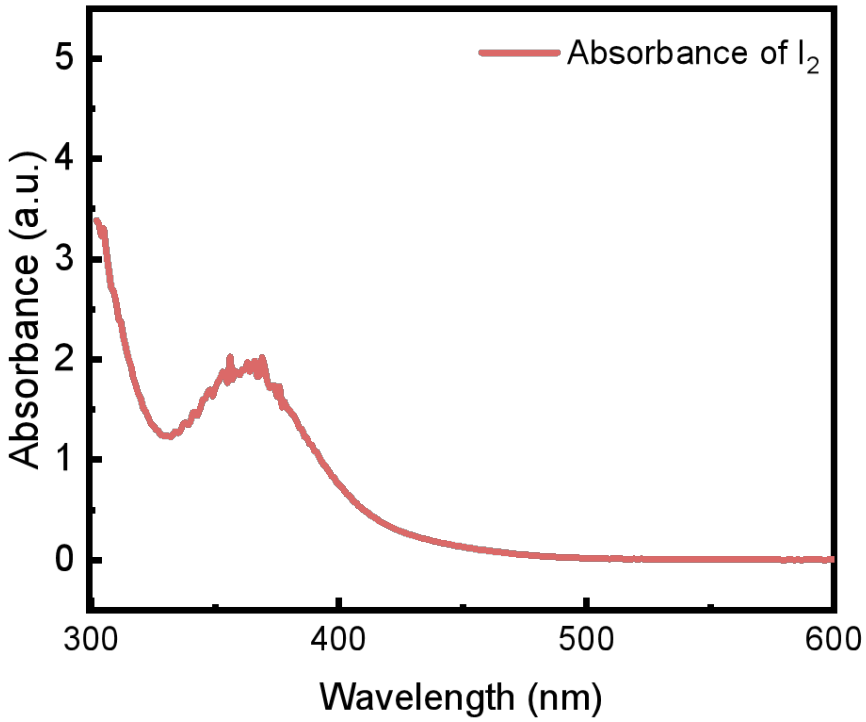

Fig. S11 Light absorption of I_3^- (typical absorbance at 350 nm) in the solution after photocatalytic reaction with addition of excess KI to detect the produced H_2O_2.[13]

Data for C-C coupling products of aryl alcohols

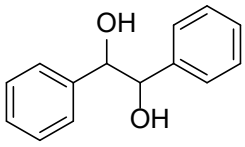

Hydrobenzoin (1a): ^{1}H NMR (500 MHz, Chloroform-*d*) δ 7.31-7.29 (m, 6H), 7.25 - 7.22 (m, 4H), 4.81 (s, 2H), 2.32 (s, 2H).

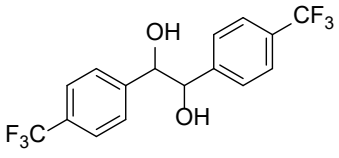

1,2-Bis[4-(trifluoromethyl)phenyl]-1,2-ethanediol (2a): ^{1}H NMR (500 MHz, DMSO-d_6) δ 7.64 (d, J = 8.1 Hz, 2H), 7.57 (d, J = 8.1 Hz, 2H), 7.50 (d, J = 8.0 Hz, 2H), 7.40 (d, J = 8.0 Hz, 2H), 5.65 (s, 1H), 5.59 (s, 1H), 4.83 (s, 1H), 4.67 (s, 1H).

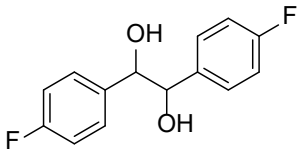

1,2-Bis(4-fluorophenyl)-1,2-ethanediol (3a): ^{1}H NMR (500 MHz, DMSO-d_6) δ 7.28 - 7.20 (m, 2H), 7.13 - 7.03 (m, 4H), 6.99 (t, J = 8.9 Hz, 2H), 5.46 (s, 1H), 5.33 (s, 1H), 4.61 (s, 1H), 4.57 (s, 1H).

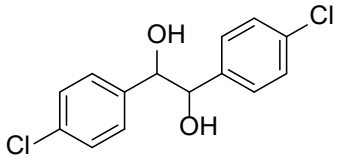

1,2-Bis(4-chlorophenyl)-1,2-ethanediol (4a): ^{1}H NMR (500 MHz, DMSO-d_6) δ 7.24 (d, J = 8.1 Hz, 4H), 7.11 (d, J = 8.2 Hz, 4H), 5.53 (s, 2H), 4.64 (s, 2H).

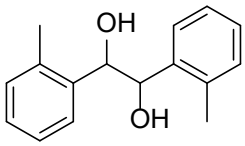

1,2-Bis(2-methylphenyl)-1,2-ethanediol (5a): ^{1}H NMR (500 MHz, DMSO-d_6) δ 7.50 (d, J = 7.9 Hz, 2H), 7.33 (dd, J = 7.0, 2.2 Hz, 2H), 7.15 - 6.98 (m, 10H), 6.87 (d, J = 7.7 Hz, 2H), 5.32 (s, 2H), 5.05 (s, 2H), 4.90 (s, 2H), 4.75 (s, 2H), 2.13 (s, 6H), 1.67 (s, 5H).

^{1}H NMR for C-C coupling products of aryl alcohols

Figure S6. ^{1}H NMR spectra of 1a recorded in Chloroform-*d*

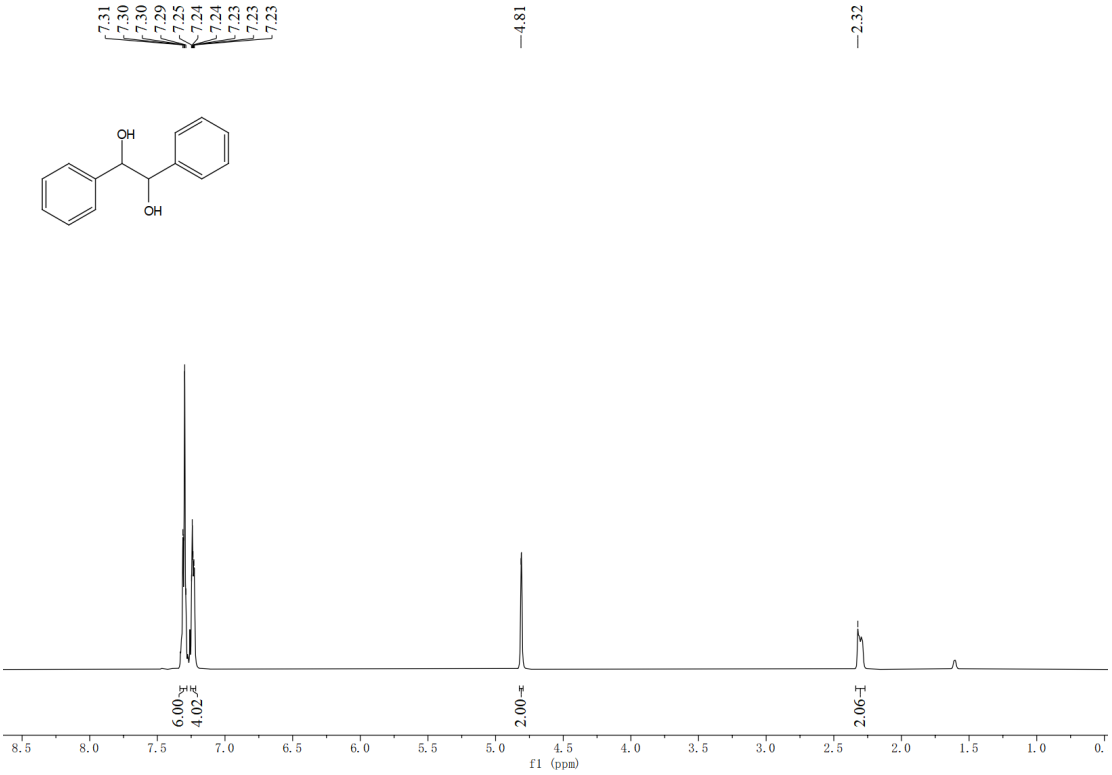

Figure S7. ^{1}H NMR spectra of 2a recorded in d_6-DMSO

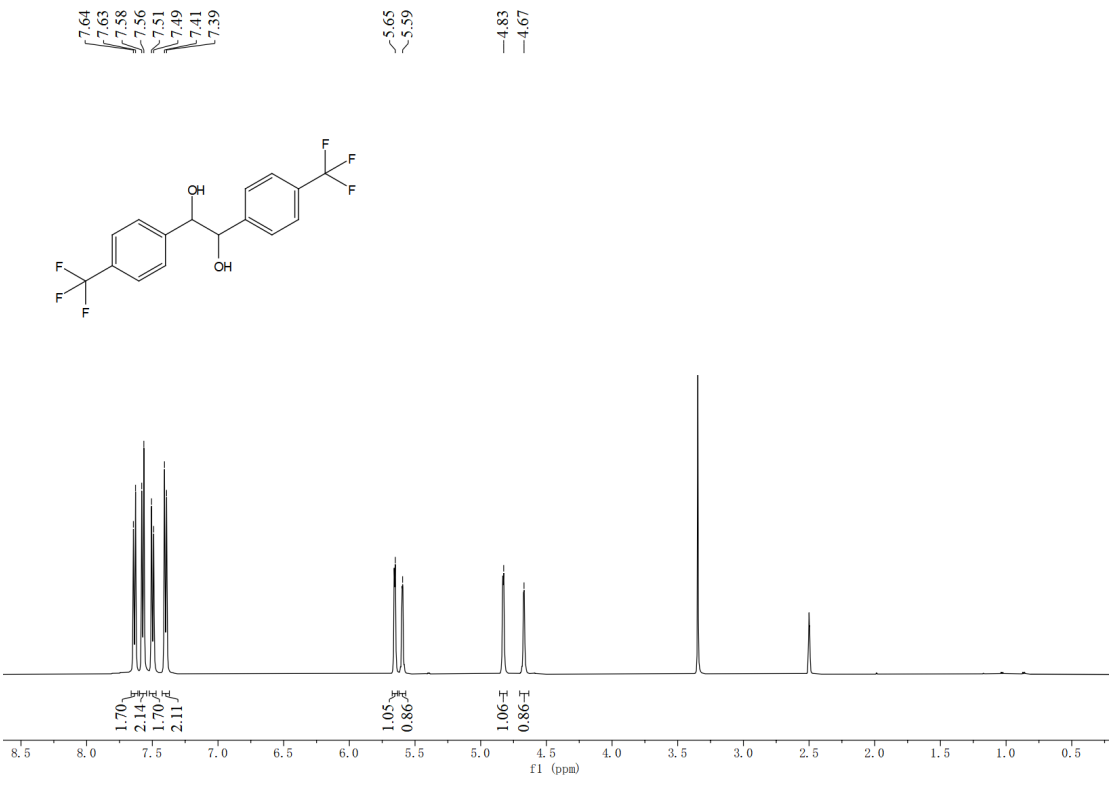

Figure S8. ^{1}H NMR spectra of 3a recorded in d_6-DMSO

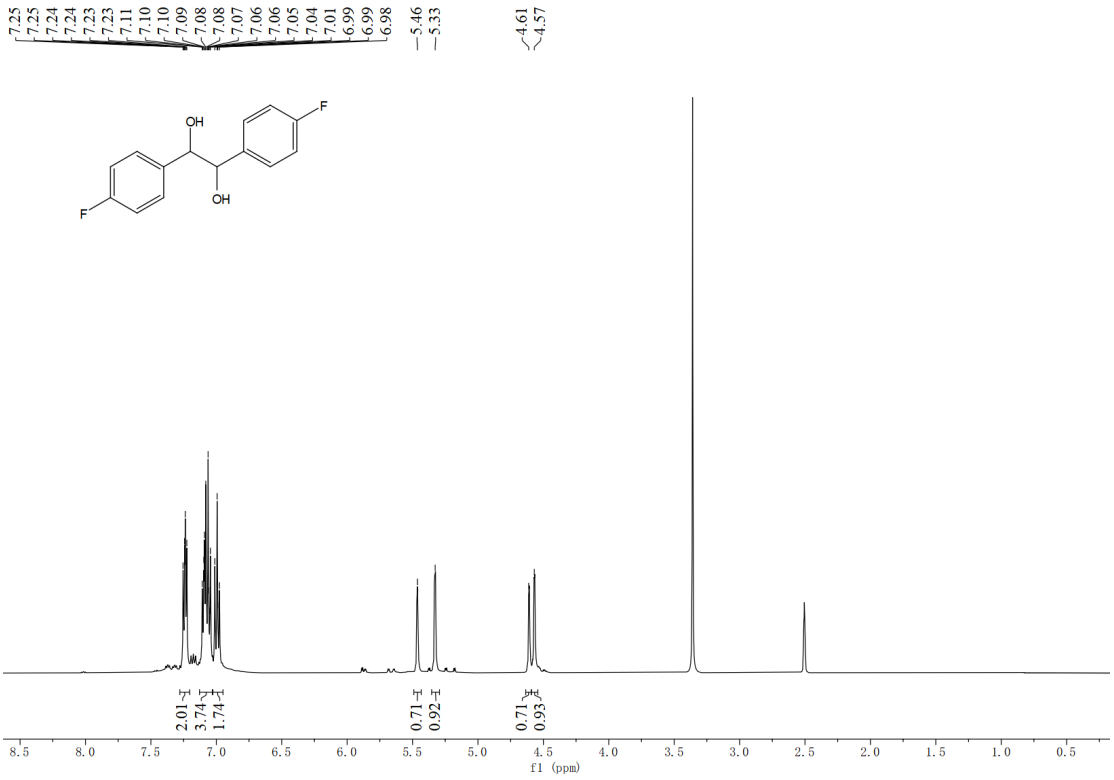

Figure S9. ^{1}H NMR spectra of 4a recorded in d_6-DMSO

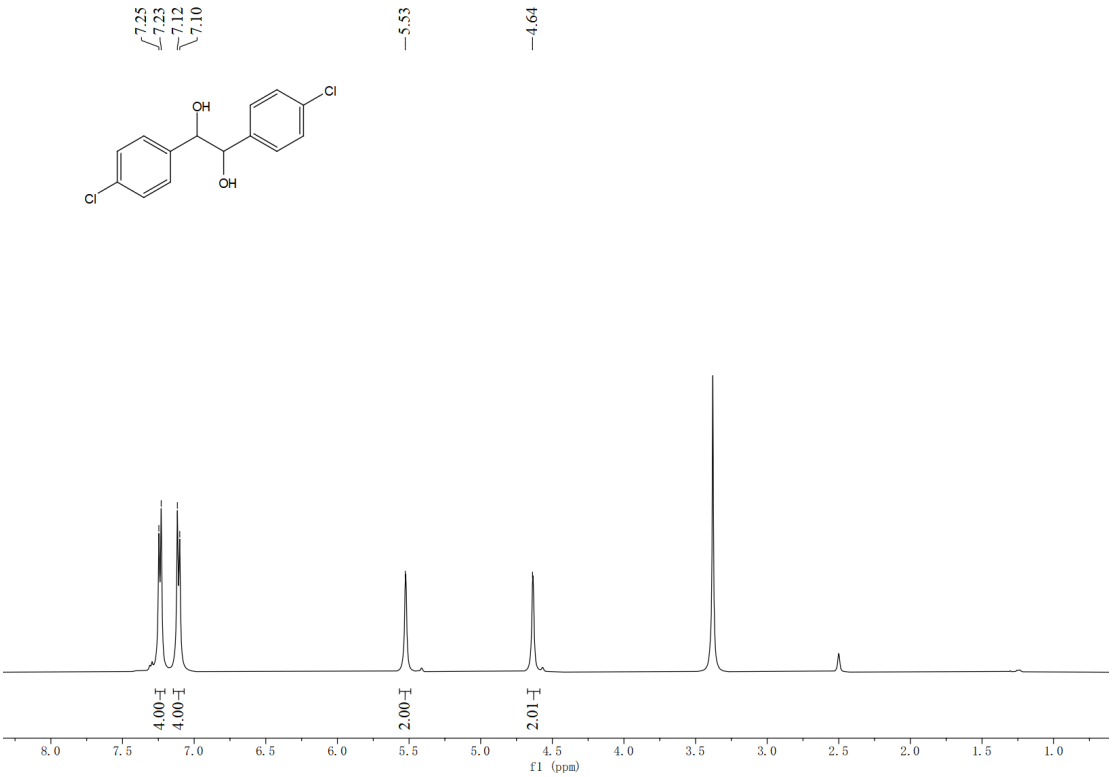

Figure S10. ^{1}H NMR spectra of 5a recorded in d_6-DMSO

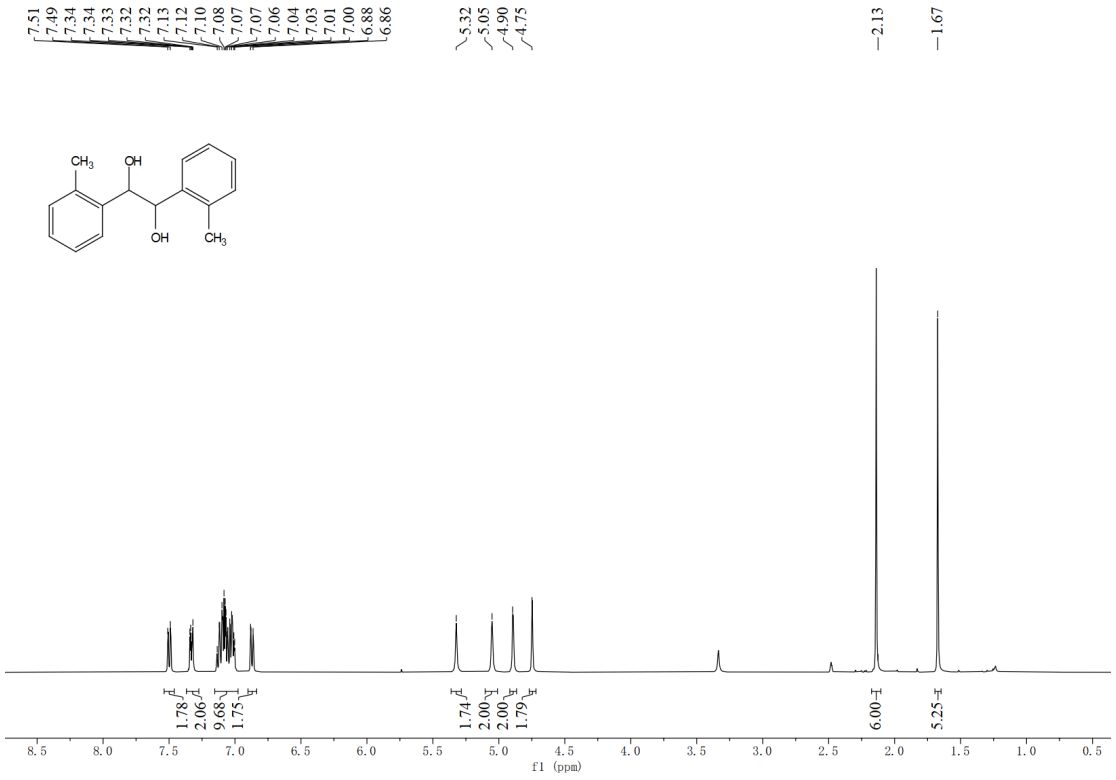

References

1 L. Yuan, Y.-H. Li, Z.-R. Tang, J. Gong and Y.-J. Xu, *J. Catal.*, 2020, **390**, 244-250.

2 S. G. Lee, M. J. Kang, M. Park, K.-j. Kim, H. Lee and H. S. Kim, *Appl. Catal., B*, 2022, **304**, 120967.

3 S. An, M. J. Kang, H. Lee and H. S. Kim, *ACS Sustainable Chem. Eng.*, 2023, **11**, 4364-4373.

4 Z. Huang, P. Sun, H. Zhang, H. Zhang, S. Zhang, Z. Chen, X. Yi and S. Xie, *ACS Catal.*, 2024, **14**, 4581-4592.

5 N. Luo, T. Hou, S. Liu, B. Zeng, J. Lu, J. Zhang, H. Li and F. Wang, *ACS Catal.*, 2019, **10**, 762-769.

6 K. P. McClelland and E. A. Weiss, *ACS Appl. Energy Mater.*, 2019, **2**, 92-96.

7 G. Han, X. Liu, Z. Cao and Y. Sun, *ACS Catal.*, 2020, **10**, 9346-9355.

8 J.-Y. Li, M.-Y. Qi and Y.-J. Xu, *Chinese J. Catal.*, 2022, **43**, 1084-1091.

9 M.-Y. Qi, Q. Lin, Z.-R. Tang and Y.-J. Xu, *Appl. Catal., B*, 2022, **307**, 121158.

10 M. Zhang, K. Li, C. Hu, K. Ma, W. Sun, X. Huang and Y. Ding, *Chinese J. Catal.*, 2023, **47**, 254-264.

11 S. Zhao, S. Song, Y. You, Y. Zhang, W. Luo, K. Han, T. Ding, Y. Tian and X. Li, *Mol. Catal.*, 2022, **528**, 112429.

12 P. Bai, X. Tong, Y. Gao and S. Xue, *Sustainable Energy Fuels*, 2020, **4**, 5488-5492.

13 H. Zhao, D. Trivedi, M. Roostaeinia, X. Yong, J. Chen, P. Kumar, J. Liu, B.-L. Su, S. Larter, M. G. Kibria and J. Hu, *Green Chem.*, 2023, **25**, 692-699.